Toward the Theory of Stochastic Condensation in Clouds. Part II: Analytical Solutions of the Gamma-Distribution Type

VITALY I. KHVOROSTYANOV

Department of Meteorology, University of Utah, Salt Lake City, Utah

JUDITH A. CURRY

Department of Aerospace Engineering Sciences, Program in Atmospheric and Oceanic Sciences, University of Colorado, Boulder, Colorado

(Manuscript received 7 August 1997, in final form 11 February 1999)

ABSTRACT

The kinetic equation of stochastic condensation derived in Part I is solved analytically under some simplifications. Analytical solutions of the gamma-distribution type are found using an analogy and methodology from quantum mechanics. In particular, formulas are derived for the index of the gamma distribution p and the relative dispersion of the droplet size spectra, which determines the rate of precipitation formation and cloud optical properties. An important feature of these solutions is that, although the equation for p includes many parameters that vary by several orders of magnitude, the expression for p leads to a dimensionless quantity of the order 1–10 for a wide variety of cloud types, and the relative dispersion σ_r is related directly to the meteorological factors (vertical velocity, turbulence coefficient, dry and moist adiabatic temperature lapse rates) and the properties of the cloud (droplet concentration and mean radius).

The following observed behavior of the cloud size spectra is explained quantitatively by the analytical solutions: narrowing of drop size spectra with increased cooling rate, and broadening of drop size spectra with increasing turbulence. The application of these solutions is illustrated using an example of a typical stratus cloud and possible applications for the convective clouds are discussed. The predictions of this solution are compared with some other models and with observations in stratus and convective clouds. These analytical solutions can serve as a basis for the parameterization of the cloud microphysical and optical properties for use in cloud models and general circulation models.

1. Introduction

During the past five decades, cloud physics and cloud optics have widely used empirical parameterizations of cloud particle size spectra such as the gamma distribution. During the past several years, the most advanced general circulation models (GCMs) have begun to incorporate sophisticated cloud microphysics models (e.g., Fowler et al. 1996) based on empirical parameterizations of cloud particle size spectra, which were included earlier only in cloud-resolving models. The parameters of these distributions are typically prescribed from observations and may vary considerably from one model to another. Ideally, these parameters should be related to the local atmospheric conditions (evaluated from the cloud bulk model or climate model) rather than prescribed uniformly over the globe.

Corresponding author address: Vitaly I. Khvorostyanov, Department of Meteorology, University of Utah, Salt Lake City, UT 84111. E-mail: vitalyk@atmos.met.utah.edu

Such an approach has been hampered by the contradiction between the theory of Maxwellian condensation, which predicts the narrowing of the drop size spectra during condensation, and observations of spectral broadening. Numerous attempts have been made to remove this contradiction, including several attempts at analytical solutions to the kinetic equations for stochastic condensation. Previous efforts at determining analytical solutions from the kinetic equations have derived a Gaussian drop size distribution. However, an analytical solution of the gamma-distribution type, which is the shape of observed drop size spectra, has remained elusive. Gamma distributions are widely used to parameterize drop size spectra, not as the solutions to the kinetic equations but as empirical parameterizations. In particular, the index of the gamma distribution, which determines the dispersion of the size spectra, was usually chosen rather arbitrarily and it was completely unclear what atmospheric parameters determine the value of index and thereby the spectral dispersion.

Numerous observations (summarized by Mason 1971; Sedunov 1974; Cotton and Anthes 1989; Prup-

pacher and Klett 1997) show that cloud droplet spectra are best described by the gamma distribution

$$f(r) = cr^p \exp(-pr/r_m), \tag{1.1}$$

where r is the drop radius, the subscript m refers to the modal value, and p is the index of gamma distribution. Gamma distributions have been used for nearly 50 years in cloud physics for parameterization of microphysical processes in cloud models (see reviews in Matveev 1984; Cotton and Anthes 1989; Pruppacher and Klett 1997) and applications to cloud optics for evaluation of the scattering and absorption coefficients in clouds (e.g., Deirmendjian 1969; Ackerman and Stephens 1987; Stephens et al. 1990; Mitchell and Arnott 1994).

The parameters of these distributions have usually been prescribed from observations. The index p is of key importance because it determines the relative dispersion of the spectra, $\sigma_r \sim (p + 1)^{-1/2}$, and thereby the cloud optical properties and the rate of precipitation formation. Values of p have usually been rather arbitrarily chosen between 1 and 10, sometimes with justification and very often without.

In the previous theories of stochastic condensation, analytical solutions have been obtained to the kinetic equations in the low-frequency approximation by Levin and Sedunov (1966), Sedunov (1974), Manton (1979), and Smirnov and Nadeykina (1986). All of the analytical solutions to the kinetic equation have been generally of the Gaussian form

$$f(r) \propto r \exp(-ar^2). \tag{1.2}$$

Comparisons of (1.2) with observations show poor agreement with the observed size spectra because (1.2) exhibits an increase that is too slow at small radii ($r < r_m$) and a decrease that is too fast at large radii, relative to observed drop size spectra.

Under certain assumptions in the low-frequency regime, we show here that the kinetic equation derived in Khvorostyanov and Curry (1999, hereafter Part I) has analytical solutions of the gamma-distribution type similar to (1.1). Analysis of the solution shows that the index p of the gamma distribution and the dispersions of the spectra can be related to the following atmospheric thermodynamic and dynamic parameters: turbulence diffusion coefficient, vertical velocity, temperature and its gradient, droplet concentration, and mean droplet radius. The predictions of this model are compared with observations in stratus clouds. Implications for the parameterization of cloud drop spectra and cloud optical and radiative properties in cloud models are discussed.

2. Analytical solution of the gamma-distribution type

For horizontally homogeneous clouds, the stochastic kinetic equation [(4.5); Part I] in the low-frequency approximation with assumption of quasi-steady supersaturation and without sources and sinks ($J = 0$) is simplified to

$$\frac{\partial f}{\partial t} + \frac{\partial}{\partial z}[(w - v(r))f] + \frac{\partial}{\partial r}\left(\frac{c}{r} w_{\text{ef}} f\right) = \left(\frac{\partial}{\partial z} + G\frac{\partial}{\partial r}\right) k_{33} \left(\frac{\partial}{\partial z} + G\frac{\partial}{\partial r}\right) f, \tag{2.1}$$

where $w = u_3$ and $w_{\text{ef}} = u_3 + w_{\text{rad}}$, and

$$c = D\frac{\rho_a}{\rho_w}\frac{c_p}{L}\frac{(\gamma_d - \gamma_s)}{4\pi DN\bar{r}}, \qquad G = \frac{c}{\bar{r}}, \tag{2.1a}$$

with variables defined in appendix B. This equation has different solutions depending on the profiles of w, k_{33}, and G, and only numerical calculations allow investigation of size spectra under various conditions. However, the following additional assumptions and simplifications allow analytical solutions to be obtained.

1) The cloud region is quasi-stationary $\partial f/\partial t = 0$.
2) Locally, $k_{33}(z) = \text{const} = k$ (chosen for simplicity, all equations below can be easily generalized to account for $dk/dz \neq 0$).
3) The vertical gradient is given by $\partial f/\partial z = \alpha f$.
4) The cloud consists of small droplets and sedimentation, $v(r)$, may be neglected relative to the vertical velocity of the air, w (the solution with account for sedimentation is considered in section 2c).

Assumption 3 above requires explanation. For example, if $\alpha(z) = b_a/z$, we can show that $f(z) = f(z_o)(z/z_o)^{b_a}$, where z_o is the cloud base height. If $df/dz = \alpha f$, it is easily shown from the definition of liquid water content $q_L = (4/3)\rho_w \pi \int r^3 f\, dr$, that $dq_L/dz = \alpha q_L$, or

$$\alpha(z) = (1/q_L)(dq_L/dz). \tag{2.2}$$

A choice of $b_\alpha = 1$ corresponds to a linear increase of droplet concentration or liquid water content with height. Generally, b_α determined from (2.2) depends on z (see Fig. 1), and the vertical gradient df/dz should include also dependence on radius. For example, if we assume that the size spectra are described by the gamma distribution with index p, modal radius r_m, and droplet concentration N, and additionally that in some layer $p(z) = \text{const}$, and $N(z) = \text{const}$, then by differentiating $f(r)$, we obtain $\alpha = (p/r_m)(dr_m/dz)(r/r_m - 1)$. If we assume $r_m \sim z^{1/3}$, then the previous equation is simplified to $\alpha = (p/3z)(r/r_m - 1)$, which includes dependencies on both r and z.

The technique described below allows such generalization and yields different solutions depending on the choice of α; however, in this paper, we consider the simplest case when $\alpha(z)$ does not depend on radius, which implies that the vertical variations in $f(r)$ in some layer caused by the vertical gradient of the droplet concentration, dN/dz, are larger than those caused by dp/dz and dr_m/dz. This assumption is reasonable for thin cloud

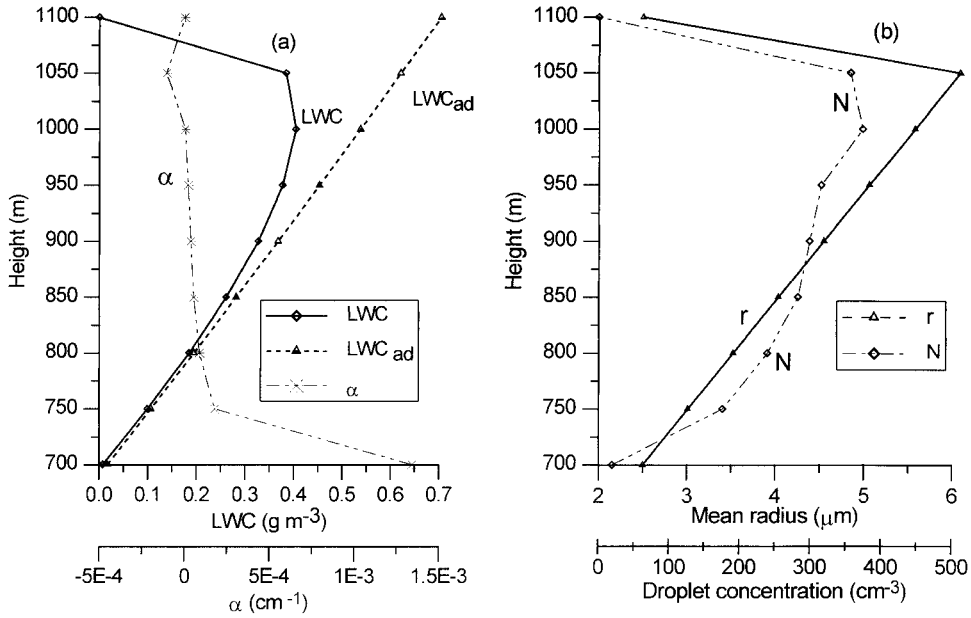

FIG. 1. Vertical profiles of liquid water content q_L, droplet concentration $N(z)$, mean radius r, and parameter $\alpha = (1/q_L)(dq_L/dz)$ for a prototype case of Arctic stratus clouds.

layers and especially for Arctic stratus where vertical variations of r_m and p are weaker than variations of N (e.g., Curry 1986).

Under these assumptions, we obtain from (2.1) the following equation:

$$G^2k\frac{d^2f}{dr^2} + \left(2G\alpha k - \frac{cw_{\text{ef}}}{r}\right)\frac{df}{dr} + \left(k\alpha^2 - w\alpha - \frac{dw}{dz} + \frac{cw_{\text{ef}}}{r^2}\right)f = 0. \quad (2.3)$$

This equation is similar in structure to the Schrödinger equation of quantum mechanics for the radial part of the wave function in the hydrogen atom. We shall therefore seek a solution of (2.3) by analogy with the hydrogen atom problem as described in Landau and Lifshitz (1958).

a. General solutions

Toward obtaining the desired form of the analytic solution, we seek a solution of the form $f(r) \sim r^p$ for small values of r and a solution of the form $f(r) \sim \exp(-\beta r)$ for large values of r. For small values of r, we retain in (2.3) only the terms that are most singular in r:

$$G^2k\frac{d^2f}{dr^2} - \frac{cw_{\text{ef}}}{r}\frac{df}{dr} + \frac{cw_{\text{ef}}}{r^2}f = 0. \quad (2.4)$$

Substituting $f(r) = r^p$ into (2.4) yields

$$p = \frac{cw_{\text{ef}}}{kG^2} = \frac{\bar{r}w_{\text{ef}}}{kG}. \quad (2.5)$$

Note that since p does not depend on α, the vertical gradients df/dz may influence the tail of the size spectra but not the index p. For large values of r, we retain in (2.3) only the terms that decrease slowly with increasing r:

$$G^2k\frac{d^2f}{dr^2} + 2G\alpha k\frac{df}{dr} + \left(k\alpha^2 - w\alpha - \frac{dw}{dz}\right)f = 0. \quad (2.6)$$

Substituting $f(r) = \exp(-\beta r)$ into (2.6), we obtain a quadratic equation for β with the following two solutions:

$$\beta_1 = \frac{\alpha}{G}(1 - \mu), \qquad \beta_2 = \frac{\alpha}{G}(1 + \mu),$$

$$\mu = \left(\frac{w}{\alpha k} + \frac{1}{\alpha^2 k}\frac{dw}{dz}\right)^{1/2}. \quad (2.7)$$

A physical solution to (2.6) requires that $\beta > 0$. Following Landau and Lifshitz (1958), the general solution to (2.3) has the form

$$f_{1,2}(r) = c_{1,2}r^p \exp(-\beta_{1,2}r)\psi_{1,2}(r). \quad (2.8)$$

Substituting (2.8) into (2.3), applying (2.2) and (2.7), and performing simple but tiresome manipulations, we obtain an equation for ψ, which for $\beta = \beta_1$ is

$$r\frac{d^2\psi}{dr^2} + \left(p + \frac{2\alpha\mu}{G}r\right)\frac{d\psi}{dr} + \frac{p\alpha}{G}(1 + \mu)\psi = 0. \quad (2.9)$$

Converting to the dimensionless variable $x = (2\alpha\mu/G)r$ and $dx = (2\alpha\mu/G)dr$, we obtain

$$x\frac{d^2\psi}{dx^2} + (p + x)\frac{d\psi}{dx} + \frac{p(\mu + 1)}{2\mu}\psi = 0. \quad (2.10)$$

This is a confluent hypergeometric equation (or Kummer equation), the solution to which, satisfying the conditions of finiteness, is the confluent hypergeometric function, $F(a, b; c)$ (Landau and Lifshitz 1958):

$$\psi_1 = c_1' F\left(\frac{p}{2\mu}(\mu + 1), p, -\frac{2\alpha\mu}{G}r\right). \quad (2.11)$$

The full solution for the droplet spectrum is then obtained from (2.8) and (2.11) to be

$$f_1(r) = c_1 r^p \exp\left[-\frac{\alpha}{G}(1 - \mu)r\right] \times F\left(\frac{p}{2\mu}(\mu + 1), p; \frac{-2\alpha\mu}{G}r\right), \quad (2.12)$$

where c_1 is a normalization factor. For $\beta = \beta_2$, the equation for ψ becomes

$$r\psi'' + \left(p - \frac{2\alpha\mu}{G}r\right)\psi' - \frac{p\alpha}{G}(\mu - 1)\psi = 0. \quad (2.13)$$

This is also a hypergeometric equation, with the solution

$$\psi_2 = c_2' F\left(\frac{p}{2\mu}(\mu - 1), p; \frac{2\alpha\mu}{G}r\right), \quad (2.14)$$

and the complete droplet size distribution function is obtained from (2.8) and (2.14) to be

$$f_2(r) = c_2 r^p \exp\left[-\frac{\alpha}{G}(1 + \mu)r\right] \times F\left(\frac{p}{2\mu}(\mu - 1), p; \frac{2\alpha\mu}{G}r\right). \quad (2.15)$$

The constants c_1 and c_2 for the distribution functions (2.12) and (2.15) can be determined using the integrals with Kummer functions described in Landau and Lifshitz (1958) (see appendix A). For solution (2.12), we obtain

$$c_1 = N\left\{\Gamma(p+1)\left[\frac{\alpha}{G}(1-\mu)\right]^{-(p+1)} \times F\left(\frac{p}{2\mu}(1+\mu), p+1, p, -\frac{2\mu}{1-\mu}\right)\right\}^{-1}, \quad (2.16)$$

where $\Gamma(x)$ is the Euler gamma function, and $F(\alpha, \beta, \gamma, x)$ is the Gaussian hypergeometric function. For (2.15) we obtain

$$c_2 = N\left\{\Gamma(p+1)\left[\frac{\alpha}{G}(1+\mu)\right]^{-(p+1)} \times F\left(\frac{p}{2\mu}(\mu-1), p+1, p, \frac{2\mu}{1+\mu}\right)\right\}^{-1}. \quad (2.17)$$

Equations (2.16) and (2.17) define c_1 and c_2 for the distribution functions, normalized to the concentration N. From appendix A, we can also determine the mean radius and water content from (A.2) and (A.3) with $n = 1, 3$. Alternatively, if the liquid water content is specified (say, from a model prognostic equation), then the liquid water content can be used to determine the constants c_1 and c_2.

Note that the existence of the two solutions can describe bimodal droplet spectra that are sometimes observed in clouds (e.g., Warner 1969a) and in chamber mixing experiments (e.g., Baker et al. 1984). This feature of these solutions resembles Manton's (1979) theory. The existence, positions, and relative strengths of the two modes are determined by the values of α, μ, G. The solution imposes some limitations on the relation among these parameters. In particular, the Kummer function can become negative or grow exponentially at large values of r for some combinations of α, μ, G.

b. Asymptotic solutions

The above expressions can be used for numerical calculations of the size spectra and their moments as described in this section. However, at least two asymptotic regimes exist where these solutions can be simplified. These asymptotic formulas can be obtained using the properties of the confluent hypergeometric function described in appendix A. Using these expressions we can consider two asymptotic regimes that simplify the solutions to (2.12) and (2.15). These regimes are determined by the term $x = 2\alpha\mu r/G$, which is the third argument of the confluent hypergeometric functions in (2.12) and (2.15).

First asymptotic regime, $x = 2\alpha\mu r/G \ll 1$. Using (A.6), we obtain from (2.12) and (2.15) the following two solutions:

$$f_1(r) = c_1 r^p \exp\left[-\frac{\alpha}{G}(1 - \mu)r\right] \quad (2.18)$$

$$f_2(r) = c_2 r^p \exp\left[-\frac{\alpha}{G}(1 + \mu)r\right]. \quad (2.19)$$

These expressions are the usual gamma distributions with index p. The condition $x = 2\alpha\mu r/G \ll 1$ implies that α should not exceed some value, $\alpha \ll G/2\mu r_{\max}$, where $r_{\max}$ is the maximum radius for which the condition holds. To estimate this value of α, we assume $r_{\max} = 10$ μm, $N \sim 200$ cm^{-3}, $\mu \sim 1$, and $G \sim 6.4$ 10^{-9}. These values give an estimation of $\alpha < 0.3$ km^{-1},

or for $q_L \sim 0.8$ g m^{-3}, a vertical gradient $dq_L/dz < 0.25$ g m^{-3} km^{-1} (from 2.2).

Thus the asymptotic formulas (2.18), (2.19) can be valid in the center of the cloud layer near the maximum value of liquid water content or in any other region where the gradient in q_L is not very large. Note, however, that when α is very small, then $\mu \gg 1$, and from the condition of finiteness, only the second solution (2.19) is valid. We call this regime the ''internal asymptotic regime,'' as it is valid in the cloud interior far from the boundaries.

Second asymptotic regime, $x = 2\alpha\mu r/G \gg 1$. Using the limit (A.5), we obtain from (2.12) and (2.15) the following two solutions:

$$f_1(r) = \tilde{c}_1 r^{\tilde{p}_1} \exp\left[-\frac{\alpha}{G}(1 + \mu)r\right],$$

$$\tilde{p}_1 = \frac{p}{2\mu}(\mu + 1) \qquad (2.20)$$

$$f_2(r) = \tilde{c}_2 r^{\tilde{p}_2} \exp\left[-\frac{\alpha}{G}(1 - \mu)r\right],$$

$$\tilde{p}_2 = \frac{p}{2\mu}(\mu - 1). \qquad (2.21)$$

This asymptotic condition should be valid for all radii, and we can rewrite it as $2\alpha\mu r_{\min}/G \gg 1$. This criterion is satisfied when α is large enough, that is, when q_L is small and its vertical gradient is large. These conditions are typical near cloud boundaries. We can estimate the region of validity of this regime by approximating the q_L profile as a linear function of height: $q_L = q_{L_0} z$, where z is height above cloud base and q_{L_0}, is a reference liquid water content. Then α can be simplified as $\alpha = (1/q_L)(dq_L/dz) = 1/z$. That is, α decreases rapidly with height above cloud base, and we can determine the following condition for z:

$$\frac{2\alpha\mu r_{\min}}{G} = \frac{2\mu r_{\min}}{Gz} \gg 1, \qquad z \ll \frac{2\mu r_{\min}}{G}. \quad (2.22)$$

Using the values $r_{\min} = 1$–1.5 μm, $\mu = 0.5$–1, $G = 1.3 \times 10^{-8}$, we obtain $z < 200$–300 m, while for $G = 2.6 \times 10^{-8}$ we obtain $z < 100$–150 m. So this asymptotic regime can be valid within several hundred meters of the upper or lower boundary of the cloud (as long as these levels do not include a maxima in the liquid water content). We refer to this regime as the ''boundary asymptotic regime'' as it is valid near cloud boundaries.

The extent of applicability of the asymptotic solution in (2.20), (2.21) is further illustrated by the following example. As the value of μ in (2.7) should be real, the following condition should be satisfied by α:

$$\frac{w}{\alpha k} + \frac{1}{\alpha^2 k}\frac{dw}{dz} > 0, \quad \text{or} \quad \alpha > -\frac{1}{w}\frac{dw}{dz} \quad \text{if } w > 0. \quad (2.23)$$

This condition allows α to be either positive or negative, depending on the vertical velocity profile in the cloud. A positive value of α indicates that q_L increases with height in the cloud, while a negative value of α indicates that q_L decreases with height in the cloud. The value of α would be zero at the maxima of q_L. The existence of vertical profiles of q_L that increase with height to a maximum value, then decrease with height above this maximum is commonly observed (see section 3) and may be caused by 1) the corresponding vertical profiles of the vertical velocity in frontal stratiform or convective clouds, 2) the entrainment of dry air into the cloud through the cloud top or turbulent mixing with the dry air near low and upper boundaries with subsequent mixing in the cloud, and 3) the vertical profiles of radiative cooling near the cloud top in stratiform clouds.

The solution (2.20) is the usual gamma distribution, where $\tilde{p}_1 = (p/2\mu)(\mu + 1)$ is the effective index of the gamma distribution. The second solution (2.21) satisfies the condition of finiteness at large r only if $\mu < 1$ for $\alpha > 0$. For the solution (2.21), the effective index $\tilde{p}_2 = (p/2\mu)(\mu - 1)$ of the gamma distribution is negative. Size spectra of the form of the inverse power law have been observed for small ice crystals (e.g., Heymsfield and Platt 1984; Ryan 1996), although this form of the size distribution is not typically observed in water clouds. Calculations such as those presented in section 2c show that the second solution (2.21) may exist in the lower cloud layer but when added to (2.20), it influences the ''tail'' of the spectrum and does not produce the secondary mode. Thus we examine primarily the first solution.

To calculate the dropsize spectra from (2.18)–(2.21), we need to define the normalization constants c_2 and c_1. Using (A.7) from appendix A, we can evaluate c_2 from the normalization to the concentration N. For (2.19) we have

$$c_2 = N[\Gamma(p + 1)]^{-1}\left[\frac{\alpha}{G}(1 + \mu)\right]^{(p+1)}. \quad (2.24)$$

For the first solution f_1 of the boundary asymptotic solution (2.20), the normalization constant is

$$\tilde{c}_2 = N\left[\Gamma\left(\frac{p}{2\mu}(1 + \mu) + 1\right)\right]^{-1}\left[\frac{\alpha}{G}(1 + \mu)\right]^{(p/2\mu)(1+\mu)+1}. \quad (2.25)$$

Using (2.19) and (2.24) for the interior asymptotic solutions and (2.20) and (2.25) for the boundary asymptotic solutions, we can easily calculate the dropsize spectra.

Using the expressions for the moments from appendix A, we can write the following expression for the liquid water content q_L and the relative dispersion of the spectrum σ_r:

$$q_L = \frac{4}{3}\pi\rho_w M^{(3)} = \frac{4}{3}\pi\rho_w N\bar{r}^3\frac{(p+2)(p+3)}{(p+1)^2}$$

$$\sigma_r = (p+1)^{-1/2}. \quad (2.26)$$

c. Solutions with account for sedimentation and generalized gamma distributions

It can be shown that sedimentation influences the tail of the size spectrum. Accounting for sedimentation under the same assumptions as used in (2.3), the kinetic equation can written in the form

$$G^2k\frac{d^2f}{dr^2} + \left(2G\alpha_l k - \frac{cw_{\text{ef}}}{r}\right)\frac{df}{dr} + \left(k\alpha_l^2 - w\alpha_l + \upsilon(r)\alpha_l + \frac{cw_{\text{ef}}}{r^2}\right)f = 0, \quad (2.27)$$

where α_l is the vertical gradient of the larger (sedimenting) droplets. We assume as usual that terminal velocity can be parameterized in the form

$$\upsilon(r) = br^{\nu}. \quad (2.28)$$

Note that the solution for the small radii, $\sim r^p$, is the same as it was for (2.3) since the most singular terms by r do not depend on $\upsilon(r)$, thus the index p is determined by (2.5). Terminal velocity for droplets of $r \sim 10$ μm is about 1 cm s^{-1}, and $\upsilon(r) \sim 5$ cm s^{-1} for the droplets with $r = 20$ μm. Thus, sedimentation becomes essential for the droplets which are far enough to the right from the modal radius and have large radii. Hence, we seek an asymptotic solution to (2.28) and retain only the main terms with the slowest decrease with r. Then we can omit the terms with inverse powers of r and to rewrite (2.27) as

$$G^2k\frac{d^2f}{dr^2} + 2G\alpha_l k\frac{df}{dr} + (k\alpha_l^2 + \alpha br^{\upsilon} - \alpha_l w)f = 0. \quad (2.29)$$

We seek a solution of the form

$$f(r) \propto \exp(-\beta r^{\lambda}), \quad (2.30)$$

which is typical of generalized gamma distributions. Substituting the relations

$$\frac{df}{dr} = f(-\beta\lambda r^{\lambda-1}),$$

$$\frac{d^2f}{dr^2} = f[(\beta\lambda)^2 r^{2(\lambda-1)} - \beta\lambda(\lambda-1)r^{\lambda-2}] \quad (2.31)$$

into (2.29) after simple manipulations we obtain the following relation:

$$G^2k[(\beta\lambda)^2 r^{2(\lambda-1)} - \beta\lambda(\lambda-1)r^{\lambda-2}] - 2G\alpha_l k\beta\lambda r^{\lambda-1} + (k\alpha_l^2 + \alpha br^{\upsilon} - \alpha_l w) = 0. \quad (2.32)$$

If $\lambda > 1$, then $2(\lambda-1) = 2\lambda - 2 > \lambda - 2$, and $2(\lambda - 1) > \lambda - 1$. Hence we retain in (2.32) at large r only the main powers of r, the largest terms are the first and fifth and we have

$$G^2k(\beta\lambda)^2 r^{2(\lambda-1)} = -\alpha_l br^{\upsilon}. \quad (2.33)$$

This equation can be satisfied only if the power law indices and coefficients are equal, thus we obtain two conditions:

$$1)\quad 2(\lambda-1) = \nu, \quad \text{or} \quad \lambda = \nu/2 + 1 \quad (2.34)$$

$$2)\quad G^2k(\beta\lambda)^2 = -\alpha_l b, \quad \text{or} \quad \beta = \frac{1}{\lambda}\left(-\frac{\alpha_l b}{G^2k}\right)^{1/2}. \quad (2.35)$$

The first condition relates the power law of the generalized gamma distribution with the power law of the terminal velocity. In particular, for the Stokes particles when $\upsilon(r) \sim r^2$, it follows from (2.34) that $\upsilon = 2$, $\lambda = 2$, and $f(r) \sim \exp(-\beta r^2)$. For the larger droplets with $r \sim 100$–500 μm, when $\upsilon(r) \sim r$ (e.g., Pruppacher and Klett 1997) and $\upsilon = 1$, we obtain $\lambda = 3/2$ and $f(r) \sim \exp(-\beta r^{3/2})$. For the next region of the larger droplets of precipitation when terminal velocity $\upsilon(r) \sim r^{1/2}$ (500 μm $< r <$ 2.5 mm), we have $\lambda = 5/4$ and $f(r) \sim \exp(-\beta r^{5/4})$. So the relation (2.34) for λ has clear physical meaning: the slower increase in terminal velocity with radius (the smaller power law) is associated with slower decrease of size spectrum with radius and the slower process of the droplet washout through precipitation.

The second condition (2.35) also has clear physical meaning. The minus sign in the brackets occurs because the vertical gradient α_l is negative for sedimenting droplets and their concentration should increase downward. Parameter β increases (size spectra decrease faster with radius) with increasing coefficient b (faster washout) and with increasing vertical gradient α_l (less compensation at a given level of the droplets loss due to sedimentation downward by the droplets gain due to sedimentation from above). Vice versa, parameter β decreases with increasing turbulence as turbulence tries to redistribute droplets in vertical and to compensate loss and gain due to sedimentation at given level. So, with account for sedimentation, the solutions to the kinetic equation have the form

$$f(r) \sim r^p \exp(-\beta r^{\lambda})\Psi(r), \quad (2.36)$$

which has the form of the generalized gamma distribution. Note that these estimations were made without accounting for collision–coalescence processes, which may change the shape of the spectra.

3. Physical interpretation of the solution

Equations (2.12), (2.15), and (2.18)–(2.21) for the droplet size distribution functions agree well with measured droplet spectra (e.g., Mason 1971; Pruppacher and Klett 1997; Cotton and Anthes 1989), because they have the functional form of the gamma distribution; that is,

they describe a power law increase of the size spectra at small values of r and an exponential decrease at large values of r. These analytical solutions allow us to determine some general properties of these parameters and hence of the drop size spectra.

a. Interpretation of the solution parameters

As shown in the previous section, the index of the gamma distribution, p, is determined from (2.5) for the first solutions (2.18) and (2.19) in the cloud interior (near the maximum liquid water content) or for the case when $\mu \sim 1$. The index of the second solution in the asymptotic regime (2.20) near the cloud boundaries is determined by the equation

$$\tilde{p}_1 = \frac{p}{2\mu}(1 + \mu), \tag{3.1}$$

with p defined by (2.5) and μ defined by (2.7). Note that $\tilde{p}_1 = p$ for $\mu = 1$.

To interpret the gamma-distribution solutions, we first analyze the index p and the parameter G, and then conduct a more complete analysis of the indices $\tilde{p}_1$ and $\tilde{p}_1$. The parameters G in (2.1a) and p in (2.5) can be written in the following form:

$$G = \frac{\rho_a}{\rho_w}\frac{c_p}{L}\frac{(\gamma_d - \gamma_s)}{4\pi N\bar{r}^2} \approx \frac{\rho_a c_p(\gamma_d - \gamma_s)}{L}\frac{\bar{r}}{q_L}$$

$$= \frac{\bar{r}}{q_L/(dq_L/dz)_{\text{ad}}} = \frac{\bar{r}}{z}\left(\frac{q_L}{q_{L,\text{ad}}}\right)^{-1} \tag{3.2}$$

$$p = \frac{\bar{r}w_{\text{ef}}}{kG} = \frac{w_{\text{ef}}}{k}\frac{L}{c_p(\gamma_d - \gamma_s)}\frac{4\pi\rho_w N\bar{r}^3}{\rho_a}$$

$$\approx \frac{w_{\text{ef}}}{k}\frac{q_L}{(dq_L/dz)} \approx \frac{w_{\text{ef}}}{k}\frac{q_L}{q_{\text{L,ad}}}z, \tag{3.3}$$

where k is the eddy diffusion coefficient and we have introduced the vertical gradient of the adiabatic liquid water content

$$\left(\frac{dq_L}{dz}\right)_{\text{ad}} = \frac{c_p}{L}(\gamma_d - \gamma_s)\rho_a. \tag{3.4}$$

As was discussed in section 4 of Part I, the effective diffusion coefficient in the space of radii is $k_r = Gk$. Equation (3.2) for G shows that 1) the diffusion coefficient k_r is proportional to the mean radius $\bar{r}$, which thereby is a ''mixing length in the space of radii'' (similar to the turbulent coefficient k proportional to the mixing length); and 2) at any given height z, k_r is inversely proportional to the liquid water ratio χ (the ratio of q_L to the adiabatic value of q_L).

Equation (3.3) for the index p also has a clear physical meaning. The indices p (and $\tilde{p}_1$) are expressed in (3.3) as the product of the three factors: 1) dynamical, w_{ef}/k; 2) adiabatic, $\chi = q_L/q_{L,\text{ad}}$; and 3) height, z. The first factor shows that the index p increases as the vertical velocity increases, narrowing the size spectrum, and p decreases as the turbulence coefficient increases, broadening the spectra. Smaller values of the adiabatic liquid water ratio χ are associated with smaller values of p and wider spectra. This is important for the interpretation of the vertical dependence of the drop spectral broadening, since in most cases χ decreases with height above cloud base but increases with cloud width (Pruppacher and Klett 1997; see Fig. 2-22). The adiabatic factor causes decrease of p and broadening of size spectra with increasing height; in particular, it explains the spectral broadening observed by Warner (1969a) and many others. The third factor in (3.3), z, causes an increase in p with height and narrowing of the spectra. Equation (3.3) provides a very simple tool for estimation of the vertical dependence of the spectral breadth from measured or calculated profiles of q_L, $\bar{r}$, w_{ef}, k, and thermodynamic parameters in a cloud.

The relationships described above are consistent with observations in clouds (e.g., Mason 1971; Pruppacher and Klett 1997; Cotton and Anthes 1989). Thus, (3.3) and (3.1) establish an analytical relationship between the index p, and hence drop spectra dispersion, on the meteorological characteristics of the atmosphere.

Consider the following atmospheric conditions typical of stratus clouds: $\gamma_s = 6$ K km^{-1}, $k = 5$ m^2 s^{-1}, and $w_{\text{ef}} = 1$–10 cm s^{-1}. As discussed in Part I, the value of w_{ef} can be estimated from the relation $\overline{w_{\text{ef}}} \sim \overline{w'q_L'}/q_L$. The values of the flux $\overline{w'q_L'}$ measured in Arctic stratus presented in Curry (1986) are always positive (except near cloud base). For the upper deck observed on 28 June 1980, the value of $\overline{w'q_L'}$ was determined to be 25–55×10^{-4} g m^{-3} m s^{-1} at $z = 818$ m with corresponding $q_L \sim 0.12$–0.2 g m^{-3}. This gives an estimate $w_{\text{ef}} \sim 12$–20 cm s^{-1}. Note that for the same deck, the covariances $\overline{w'w'} \sim 0.1$–0.2 m^2 s^{-1} (Curry et al. 1988), that is, $w' \sim (\overline{w'w'})^{1/2} \sim 33$–$45$ cm s^{-1}, which is larger than the previous estimate for w_{ef}. This is in agreement with the discussion of the covariances in Part I, which showed that the correlation function $\overline{w'f'}$ or $\overline{w'S'}$ due to the phase shift between them by τ_f should be smaller than the autocovariance $\overline{w'w'}$; here w_{ef} should be smaller than w'. However, w_{ef} should be still much greater than the synoptic-scale average $w_{\text{syn}} \sim 0.5$–1 cm s^{-1}.

The values of parameters p and G calculated from (3.2) and (3.3) are presented in Tables 1 and 2. Table 2 shows that the values of p for the ''interior cloud'' solution (2.18) and (2.19) range from 2 to 8 for $w_{\text{ef}} = 10$ cm s^{-1} in a cloud with mean radius $\bar{r} = 5$ μm and

TABLE 1. Parameter G (10^{-8}) for $\gamma_s = 6$ K km^{-1} and various values of droplet concentrations N and mean radii $\bar{r}$.

	N, cm^{-3}		
$\bar{r}$, μm	10^2	2×10^2	4×10^2
5	5.1	2.6	1.27
10	1.3	0.64	0.32

TABLE 2. Parameters p of gamma distribution for $k = 5$ m^2 s^{-1}, $\gamma_s = 6$ K km^{-1}, with various droplet concentrations N, mean radii $\bar{r}$, and vertical velocities w_{ef}.

	N, cm^{-3}		
$\bar{r}$	10^2	2×10^2	4×10^2
	$w_{ef} = 1$ cm s^{-1}		
5 μm	0.2	0.4	0.8
10 μm	1.6	3.2	6.4
	$w_{ef} = 10$ cm s^{-1}		
5 μm	2	4	8
10μm	16	32	64

TABLE 3. Relative dispersions $\sigma_r = (p + 1)^{-1/2}$ of the gamma distribution for various droplet concentrations N, mean radii $\bar{r}$, and w_{ef} for the same parameters used in Table 2.

	N, cm^{-3}		
$\bar{r}$	10^2	2×10^2	4×10^2
	$w_{ef} = 1$ cm s^{-1}		
5 μm	0.91	0.84	0.74
10 μm	0.62	0.49	0.37
	$w_{ef} = 10$ cm s^{-1}		
5 μm	0.58	0.45	0.33
10 μm	0.24	0.17	0.12

droplet concentration $N = 1$–4×10^2 cm^{-3}, typical for continental, summertime Arctic stratus clouds (Curry 1986) or some types of marine clouds near the coast (Noonkester 1984). This value of p corresponds to dispersions of the spectra $\sigma_r \sim 0.33$–0.58 (Table 3), which is close to values observed in the central layers of such clouds. For values of $\bar{r} = 10$ μm, typical of marine stratus clouds, the values of p increase; however, since typical drop concentrations are usually $N = 1$–2 10^2 cm^{-3} for these clouds, values of p would not normally exceed $p = 8$–16 for this cloud type and would be less for smaller values of w_{ef}. Thus, from Table 2 we see that the spectra narrows with increasing droplet concentration and mean radius. If the value of the turbulence coefficient is $k = 10$ m^2 s^{-1} or the maximum effective vertical velocity is 5 cm s^{-1}, the values of p in Table 2 would be twice as small.

These tables show that for $w_{ef} = 1$–2 cm s^{-1}, as could be evaluated from the large-scale divergence (i.e., with the averaging over the large areas), the values of p are too small ($p < 1$ for $\bar{r} = 5$ μm), and the dispersions are too large compared to the local observations. The problem of correspondence of the local size spectra and those averaged over the large cloud areas has been widely discussed in the literature, and it was found that the scale of averaging influences the index p: the local (measured over the horizontal scales $L_x \sim 30$–100 m) spectra are usually narrow, with $p = 6$, $\sigma_r = 0.38$ to $p = 10$, $\sigma_r = 0.30$ (e.g., Aleksandrov and Yudin 1979; Curry 1986). However, the dispersions increase and the indices p decrease to $p \sim 1$–2 ($\sigma_r = 0.58$–0.7) with increasing scale of averaging, ($L_x \sim$ a few kilometers) or with averaging over many clouds (e.g., Mason 1971; Sedunov 1974). This effect of averaging is clearly seen from the data by Noonkester (1984) for marine stratocumulus shown in Table 4, which illustrates the increase in σ_r (artificial ''broadening'' of the spectra) with averaging over the scale 6.44 km ($\sigma_{r,\mathrm{all}}$) as compared to the local spectra averaged over 0.529 km ($\sigma_{r,\mathrm{loc}}$). This impact of averaging on the width of the size spectra is described by (3.3) since $p \sim w_{ef}$, which decreases with increasing scale of averaging. Note, however, that the cloud optical and radiative properties and the rate of precipitation formation are determined by the local ($L_x \sim 50$–100 m) size spectra, hence the local values $p = 6$–10 with $\sigma_r = 0.3$–0.4 are representative and should be used for the parameterizations.

Since the large-scale models with the horizontal grid spacing ~100–400 km produce $w_{ef} \leq 1$–2 cm s^{-1} we address the problem of the subgrid parameterization of w_{ef}. One possible solution to this problem was suggested by Dmitrieva-Arrago and Akimov (1998) in a general circulation model with prognostic equations for q_L and dewpoint deficit, and a prescribed value of p. The subgrid value of w_{ef} for stratiform clouds is defined in this GCM as the minimum velocity required to support the falling droplets with radii smaller than some threshold value, say, 40 μm. Assuming Stokes's velocities gives $w_{ef} \approx 20$ cm s^{-1}, which is comparable to the estimation above from the covariances. With $k \sim 10$ m^2 s^{-1}, values in Table 2 would give reasonable values of $p \sim 5$–10, so the method developed here can be used in such GCMs with parameterizations of subgrid w_{ef} similar to Dmitrieva-Arrago and Akimov (1998).

An important feature of the solutions for p obtained

TABLE 4. Observed relative dispersions, $\sigma_r = (p + 1)^{-1/2} = (\sigma_{\mathrm{abs}}/r\bar{r})$, and corresponding indices p in low stratus clouds.

(a) Arctic summertime stratus (Curry 1986)

Deck, date	Height, m	q_L, g m^{-3}	σ_r	p
20 Jun 1980	289 (top)	0.02	0.39	5.6
	241	0.42	0.30	10.1
	183	0.35	0.31	9.4
	91	0.20	0.36	6.7
28 Jun 1980	1082 (top)	0.03	0.38	5.9
	940	0.30	0.33	8.2
	819	0.10	0.40	5.3
	696 (base)	0.02	0.51	2.8

(b) California coastal stratus (Noonkester 1984); $\sigma_{r\mathrm{loc}}$ and p_{loc} are averages over local paths of 529 m, $\sigma_{r\mathrm{all}}$ and p_{all} are averages over all path of 6.44 km.

Date	Height above cloud base, m	q_L, g m^{-3}	$\sigma_{r\mathrm{loc}}/\sigma_{r\mathrm{all}}$	$p_{\mathrm{loc}}/p_{\mathrm{all}}$
29 May 1981	274 (top)	0.288	0.42/0.67	4.7/1.2
	167	0.217	0.21/0.66	21.7/1.3
	18	0.034	0.57/0.89	2.1/0.3
18 Aug 1981	222 (top)	0.263	0.79/0.94	0.6/0.13
	121	0.199	0.37/0.78	6.3/0.6
	17	0.037	0.56/0.81	2.2/0.5

here is that although (3.3) p includes many parameters that vary by several orders of magnitude, the expression for p leads to a dimensionless quantity of order 1–10 for a wide variety of stratus cloud types, and the relative dispersion is related now directly to the meteorological factors (w, γ_d, k), the properties of the cloud (N, $\overline{r}$), and fundamental atmospheric constants.

For convective clouds, typical values of vertical velocity are $w \sim 2.0$–5.0 m s^{-1}; that is, 20–30 times larger than values used in Table 2 for stratiform clouds. Although the values of the turbulence coefficient for cumulus can be about 10–20 times larger than those for stratus clouds, this shows that the values of p should be larger and spectra narrower in cumulus, which is expected since the processes in the vigorous updrafts are closer to the regular condensation.

An example is given using data presented by Austin et al. (1985) of microphysical measurements in shallow convective clouds obtained simultaneously at two levels by two aircrafts separated by 800 m in height. The size spectra at lower level in the middle of the cloud have the $\overline{r} = 7$–8 μm, $\sigma_{\text{abs}} = 0.6$–$1.0$ μm, $\sigma_r = 0.2$–0.3, and $p = 13$–25. At the higher level, near the top, $\overline{r} = 8$–8.5 μm, $\sigma_{\text{abs}} = 0.5$–$0.7$ μm, $\sigma_r = 0.17$–0.21, and $p = 22$–35. So the size spectra narrows with height, in contrast to the convective cloud observed by Warner (1969a). A similar estimation can be obtained for convective clouds; assuming $w_{\text{ef}} = 2$ m s^{-1}, $k = 30$ m^2 s^{-1}, $\chi = 0.7$, and $z = 700$ m, we obtain $p = 35$, $\sigma_r = 0.17$. While this is a very rough estimation, it shows that this approach gives the correct order of magnitude for convective clouds.

Equation (3.3) shows that the size spectra may become broader or narrower with increasing height, depending on the behavior of $\zeta = (w_{\text{ef}}/k)\chi$. If ζ decreases with height faster than z, say as $z^{-3/2}$, we obtain $p \sim z\zeta \sim z^{-1/2}$, so p decreases and dispersion increases with height, in agreement with observations by Warner (1969a) near cloud bottom. For ζ decreasing with height slower than z, such as closer to cloud tops, the situation is reversed, that is, p increases and dispersions decrease with height.

Note that the entrainment processes in cumulus or near the tops of stratocumulus can be easily accounted for in this approach by addition into the right-hand side of the kinetic equations (2.1), (2.3) of the term $-\tau_m^{-1} \times f$, with τ_m being the characteristic mixing time. Then the two solutions (2.7) for $\beta_{1,2}$ are modified,

$$\beta_{1,2} = \frac{\alpha}{G}\left[1 \pm \left(\frac{\tau_m^{-1}}{k\alpha^2} + \frac{w}{k\alpha} + \frac{1}{k\alpha^2}\frac{dw}{dz}\right)^{1/2}\right], \quad \text{(3.4a)}$$

and can give the bimodal distributions. Equation (3.4a) shows that with decreasing mixing time, τ_m^{-1} increases and leads to the larger separation of the modes and to broader spectra. Recall that one of Manton's (1979) results was that the size spectra of each single mode was too narrow and only their bimodal superposition could ensure the dispersion growing with height at a rate comparable to the measured values (Warner 1969a). A bimodal superposition of the gamma distributions considered here may also provide sufficient dispersion for the case of cumulus clouds.

Equation (3.3) for p shows also that there is a temperature dependence of the drop size spectra. Liquid water clouds can occur over a large range of temperatures, particularly since supercooled liquid clouds are observed at temperatures as low as $-35°$ to -39°C (Pruppacher and Klett 1997). According to (3.3), drop size spectra narrow at colder temperatures. When the temperature decreases, the value of the moist adiabatic lapse rate γ_s approaches the dry adiabat γ_d; therefore the difference $(\gamma_d - \gamma_s)$ in the denominator of (3.3) decreases and p increases. Hence, the size spectra narrows with decreasing temperature. For example, for a low-level cloud at $T = -20$°C, the difference $(\gamma_d - \gamma_s) \approx 1.5$ K km^{-1} instead $(\gamma_d - \gamma_s) \approx 4$ K km^{-1} at $T = 0$°C, so the values of p in Table 2 should be 2.7 times larger for $T = -20$°C. This increase may be partially compensated by a decrease in w_{ef}.

This temperature dependence explains narrowing of the spectra with decreasing temperature observed in Arctic summertime clouds (Herman and Curry 1984; Tsay and Jayaweera 1984). In the summertime Arctic altostratus ($T = -12°$ to -15°C), $\overline{r} = 3.8$ μm and $r_{95} = 9$ μm, while in stratus ($T = 1°$–6°C), $\overline{r} = 4.5$–6 μm, and $r_{95} = 12$–18 μm, where r_{95} is the right boundary of the interval containing 95% of the droplets. This narrowing of the spectra with decreasing temperature leads to both the relative colloidal stability of upper clouds (as narrowing of the spectra prevents coagulation) and the decreasing probability of droplet freezing (which is proportional to the drop volume).

b. Applications of the solution

To illustrate the analytical solutions and evolution of the droplet spectra below the maximum in q_L, we consider the following characteristics typical of low stratus clouds and close to the Arctic stratus observed on 28 June 1980, upper layer (Curry 1986). The vertical profile of q_L is approximated by a parabolic profile of the form $q_L(z) \sim q_{L,\max} \times (z/H)^a \times (1 - z/H)^b$, with H being the cloud depth; q_L and the parameter α are presented in Fig. 1. Cloud boundaries are at 700 and 1100 m and the maximum value $q_{L,\max} = 0.4$ g m^{-3} is located at ~1000 m. The vertical profile of the mean radius is chosen such that $\overline{r} = 2.5$ μm at the cloud bottom and linearly increases to $\overline{r} = 6$ μm at the cloud top. The vertical profile of the droplet concentration N calculated using these values of q_L and $\overline{r}$ is also presented in Fig. 1 and exhibits the fastest increase above the base with much slower increase in midcloud. Such profiles are also in agreement with the results of large eddy simulations of stratocumulus (Feingold et al. 1994), averaged over the domain.

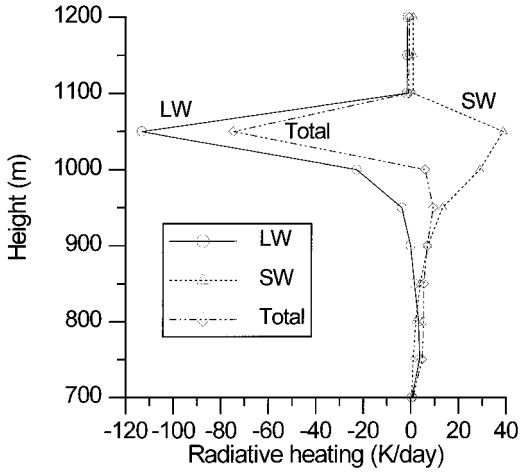

FIG. 2. Vertical profiles of longwave, shortwave, and total radiative heating rates for the cloud shown in Fig. 1.

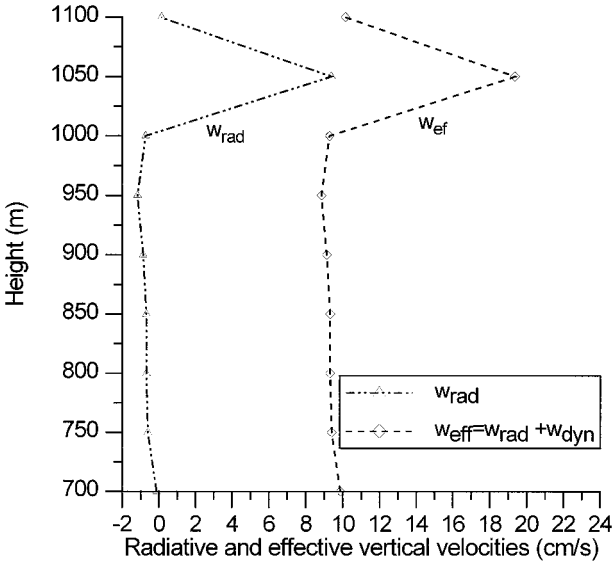

FIG. 3. Vertical profiles of the effective-radiative vertical velocities $w_{rad} = w_{long} + w_{short}$ calculated with (2.8) of Part I for the cloud shown in Figs. 1 and 2 with account for the both longwave and shortwave cooling/heating, and the total effective velocity $w_{eff} = w_{dyn} + w_{rad}$, where $w_{dyn} = 1$ cm s^{-1}.

To investigate the effect of vertical velocity, turbulence, and radiation on the drop size spectra, we examine four different cases, using the definition of effective vertical velocity $w_{ef} = w_{rad} + w_{dyn}$ derived in Part I, section 2a. The four cases are the following: 1) w_{rad} is determined by accounting for the longwave cooling rate only, $w_{dyn} = 1$ cm s^{-1}, and $k = 5$ m^2 s^{-1}; 2) w_{rad} is determined by accounting for longwave cooling only, $w_{dyn} = 10$ cm s^{-1}, and $k = 5$ m^2 s^{-1}; 3) $w_{rad} = 0$, $w_{dyn} = 15$ cm s^{-1}, and $k = 5$ m^2 s^{-1}; and 4) w_{rad} is determined by accounting for longwave cooling only, $w_{dyn} = 10$ cm s^{-1}, and $k = 10$ m^2 s^{-1}. These variations allow examination of the individual effects of w, k, and radiation on the drop size spectra.

Radiative heating rates are calculated as described in Khvorostyanov (1995) using input variables consistent with the observed Arctic stratus clouds from Fig. 1. Calculated profiles of radiative heating rates presented in Fig. 2 show maximum longwave cooling of -120 K day^{-1} and solar heating of $\sim$40 K day^{-1}, which is in a good agreement with those determined from measurements of this cloud deck (Herman and Curry 1984; Curry 1986). Corresponding radiative-effective vertical velocities (Fig. 3) exhibit strong maxima at heights 50–100 m below cloud top, equivalent to updrafts of 5–8 cm s^{-1} for the longwave cooling and downdrafts of -3 cm s^{-1} for solar heating, and almost vanish in the lower half of the cloud, where the dynamic velocity plays the major role. The value of parameter α (Fig. 1) shows a strong maximum near cloud base, sharply decreases upward in the lowest 50 m of the cloud, then continues to decrease much more slowly until it reaches zero at a height of 1000 m and becomes negative above this level. The values of parameter μ calculated from (2.7) and shown in Fig. 4 exhibit a monotonic increase upward from about 0.2–0.6 near cloud bottom to values $\mu = 4$–5.5 within 200–300 m above cloud base, with values of μ significantly increasing above 900 m where radiative-effective velocities and their gradients increase. The indices p of the general solutions (Fig. 5) for the case with $w_{dyn} = 1$ cm s^{-1} (synoptic scale) do not exceed 1–2 in the whole cloud but reach 20 in the thin layer of maximum radiative cooling near 1050 m. The values of p for $w_{dyn} = 10$–15 cm s^{-1} are much greater and closer to the local observations. They also exhibit an increase from the cloud bottom with the val-

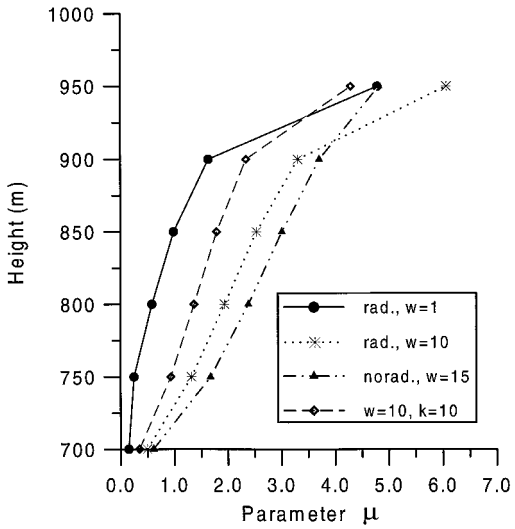

FIG. 4. Vertical profiles of the parameter μ in the analytical solutions calculated with (2.7) for four cases: 1) $w_{ef} = w_{dyn} + w_{rad}$; $w_{dyn} = 1$ cm s^{-1}, and w_{rad} calculated with (2.8) of Part I with account for the longwave cooling only; $k = 5$ m^2 s^{-1}; 2) same as case 1, but $w_{dyn} = 10$ cm s^{-1}; 3) same as case 1, but $w_{dyn} = 15$ cm s^{-1} and $w_{rad} = 0$; 4) same as case 2, but $k = 10$ m^2 s^{-1}.

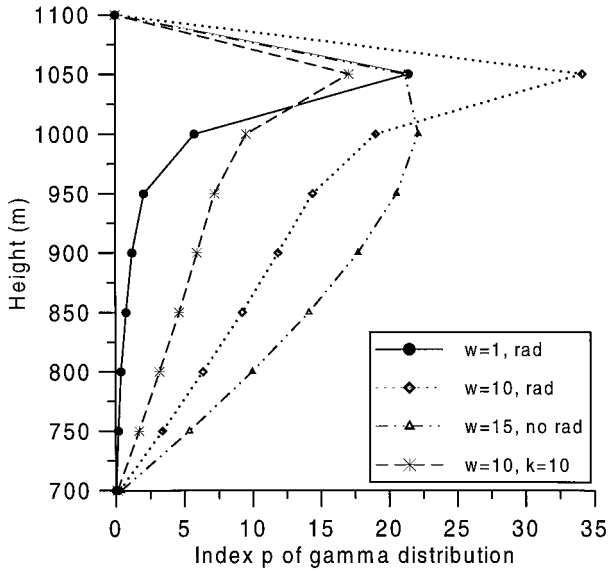

FIG. 5. Vertical profiles of the indices p of gamma distributions defined by (3.3) for the same four cases as in Fig. 4. Hereafter the values of w_{dyn} and k are shown in figures; ''rad'' and ''norad'' mean calculations with and without account for the radiation.

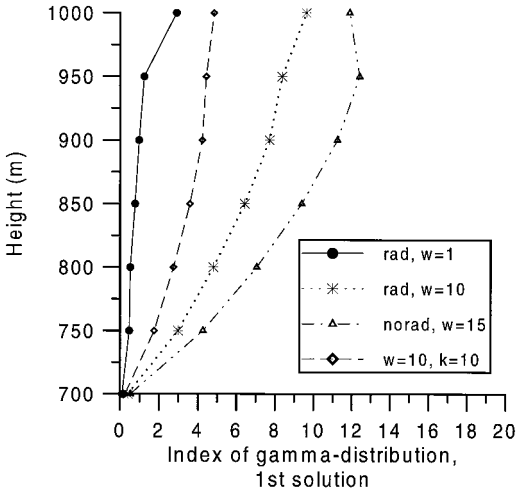

FIG. 6. Vertical profiles of the indices $\tilde{p}_1$ of gamma distributions defined by (3.1) for the first asymptotic solution (2.20) (boundary asymptotic regime) for the same four cases as in Fig. 4.

ues 5–15 in midcloud depth, reach maximum values of 20–35 near the maximum q_L, and then decrease upward toward the cloud top. For the cases with $w_{rad} > 0$, this increase is especially rapid near the maximum q_L where w_{rad} is maximum.

The indices $\tilde{p}_1$ of the gamma distribution for the first solution (2.20) calculated with (3.1) (Fig. 6) also increase upward from the cloud bottom but more slowly than the indices p. This is explained by the behavior of the parameter μ, which is greater for the larger vertical velocities and smaller turbulence coefficient; that is, μ shows the opposite behavior from parameter p in (3.3), thereby partially counteracting the effects of vertical velocities and turbulence on $\tilde{p}_1$ and size spectra as seen from (3.1). As discussed in section 2, the asymptotic solutions (2.20) with indices $\tilde{p}_1$ are valid only in the lower layer of ~100–200 m, while the larger indices p (Fig. 5) are more representative of the spectral dispersions in the upper half of the cloud. It is seen from Figs. 5 and 6 that values of both p and $\tilde{p}_1$ increase with increasing vertical velocity and decrease with increasing turbulence.

An example of the size spectra in the lower part of the cloud calculated with (2.20) is presented in Fig. 7. The shape and the general behavior of the spectra are in reasonable agreement with those typically observed in clouds. The calculated size spectra can be compared to those measured on 28 June 1980 in stratus (Herman and Curry 1984, their Table 2). There were five aircraft passes through this cloud deck at various altitudes. Although the measured spectra are slightly different at various times, they exhibit some common features. 1) In lower 100–150 m, the spectra are monomodal, with distinct maxima in the size bins at 1.6 and 3.1 μm, and rapidly decrease in the bins 4.7–6.3 μm. 2) At higher altitudes, the maxima in the first bins become smaller but still exist, and the new maxima occur in the bins 6.3–9.4 μm with the minimum at 4.7 μm, so the mean radius grows with height and the spectra exhibit features of bimodality. We see that calculated spectra (Fig. 7) generally reproduce the shape of the measured spectra: (i) the fast increase of $f(r)$ in the region from 0 to 1–2 μm caused by the high value $p \sim 5$–10, (ii) slower exponential tail, (iii) displacement of the maximum to the lager radii with height, and (iv) simultaneous decrease of the relative dispersion σ_r upward (see Table 4 for the measured σ_r and Figs. 8 and 9 for calculated σ_r). The feature of bimodality is not reproduced in Fig. 7, as accounted for by only one mode in the analytical

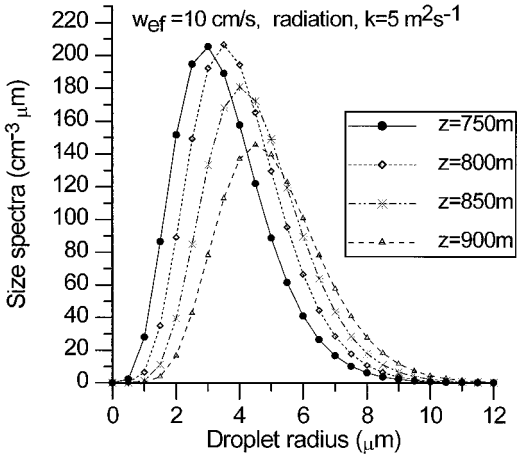

FIG. 7. Evolution of the droplet size spectra above cloud base calculated with the first asymptotic solution (2.20) for the case with $w = 10$ cm s^{-1}, w_{rad} as in Fig. 2, $k = 5$ m^2 s^{-1}, normalized to the concentration $N(z)$ shown in Fig. 1.

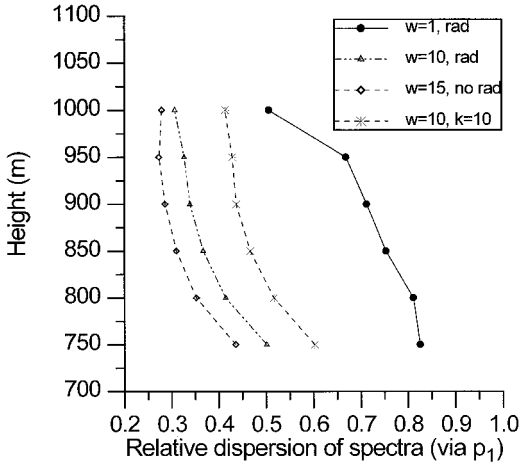

FIG. 8. Vertical profiles of the relative dispersions of the size spectra for the first asymptotic solution (2.20) for the same four cases as in Fig. 4 calculated with indices $\tilde{p}_1$.

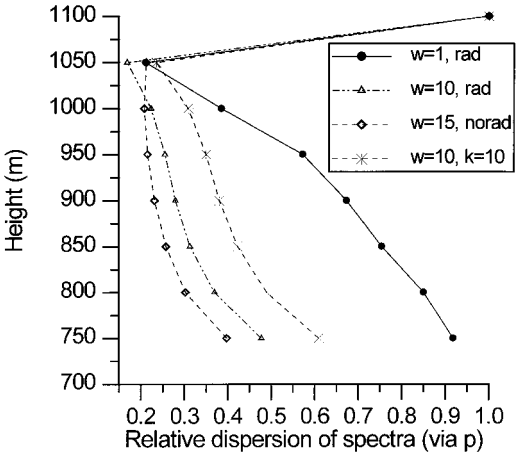

FIG. 9. Vertical profiles of the relative dispersions of the size spectra for the same four cases as in Fig. 4 calculated with indices p defined by (3.3).

solutions. This bimodality is probably caused by the mixing with the entrained dry air from above and can be reproduced in this model by using a superposition of the solutions with the two exponents $\beta_{1,2}$ in (3.4a) with appropriate mixing time τ_m.

c. Comparison with some previous theories and observations

The theory of stochastic condensation and the stochastic kinetic equations have been criticized by Warner (1969b), Bartlett and Jonas (1972), and others, who modeled the impact of turbulence on the size spectrum as random fluctuations of a cloud parcel using Lagrangian parcel models. They found that turbulence within a cloud is unable to account for the observed drop size distributions. It was noted by Stepanov (1975) and Voloschuk and Sedunov (1977) that the kinetic equation under some conditions does not cause further broadening of the spectra with time. We consider here in more detail the correspondence between the approach based on the kinetic equation and the Lagrangian parcel models. We will show that there is no contradiction between these two approaches and that Warner (1969b) and Bartlett and Jonas (1972) considered a particular case of stochastic condensation.

As we see from the low-frequency form of the kinetic equation (2.1), the effect of turbulence vanishes when the right-hand side of the equation is zero, and (2.1) converts into the equation of regular condensation (2.1). The right-hand side of (2.1) can be zero if either

$$k = 0 \quad \text{or} \tag{3.5}$$

$$\left(\frac{\partial}{\partial z} + G\frac{\partial}{\partial r}\right) f = 0. \tag{3.6}$$

Thus, condition (3.6) can be regarded as equivalent to the condition of zero turbulence (3.5). Equation (3.6) can be rewritten as

$$\frac{\partial f}{\partial z} = -G\frac{\partial f}{\partial r}. \tag{3.7}$$

Multiplying (3.7) by $(4\pi/3)\rho_w r^3$ and integrating, we obtain

$$\frac{dq_L}{dz} = -\frac{4\pi}{3}\rho_w G \int_0^\infty r^3 \frac{\partial f}{\partial r}\, dr = 4\pi G \rho_w N \overline{r^2}$$

$$\approx 4\pi G \rho_w N \bar{r}^2. \tag{3.8}$$

The last approximate relation is based on the fact that $\overline{r^2}$ is usually only slightly (by 10%–20%) larger than $\bar{r}^2$.

To interpret (3.8), we express G in terms of the vertical gradient of the adiabatic liquid water content defined by (3.4). Substituting (3.4) into the first of the relations (3.2), we obtain

$$G = \left(\frac{dq_L}{dz}\right)_{\text{ad}} \frac{1}{4\pi\rho_w N \bar{r}^2}. \tag{3.9}$$

Thus, the parameter G relates the vertical gradient of the adiabatic liquid water content to the effective area of the droplets per unit volume; that is, G characterizes the rate of absorption by the droplets of vapor excess released during adiabatic lifting. Substituting (3.9) for G into (3.8) and incorporating (2.2), we obtain the following relation:

$$\frac{dq_L}{dz} = 4\pi G \rho_w N \bar{r}^2 = \left(\frac{dq_L}{dz}\right)_{\text{ad}}. \tag{3.10}$$

Equation (3.10) shows that the condition (3.6) corresponds to the adiabatic q_L or, as shown by (3.5) and (3.6), this is equivalent to $k = 0$. So we see that turbulence does not influence the drop size spectrum if the vertical profile of q_L corresponds to the adiabatic value.

In the simulations made by Warner (1969b) and Bartlett and Jonas (1972) using Lagrangian parcel models, moist adiabatic ascent was assumed and adiabatic liquid water contents were derived. This corresponds to the absence of turbulence, therefore small broadening of the spectra was obtained in these parcel models (probably due to the numerical dispersion). Hence, there is no contradiction between the treatment of stochastic condensation process as described here and the Lagrangian parcel models, which correspond to the condition of equilibrium (3.6). This condition along with the physical meaning of parameter G as described by (3.9) means that any vertical displacement in the cloud is accompanied by a change in the dropsize spectrum. Displacements of parcels in regions of the clouds that have adiabatic liquid water profiles will not lead to the broadening of the drop size spectra, and the droplet radius will be a function of the height and the cloud will be in some equilibrium state. However, liquid water content in a cloud is typically much less than its adiabatic value and condition (3.10) is not satisfied. This departure of the cloud liquid water content from the adiabatic profile increasing upward will result in the evolution of the size spectra according to the kinetic equation of stochastic condensation. Since the ratio $\chi = q_L/q_{L,\mathrm{ad}}$ usually decreases upward, the applicability of the parcel models without entrainment and with adiabatic gradients becomes more limited with increasing height above cloud base.

Considine and Curry (1996) used a simple statistical model to derive a drop size spectra that has the shape of a modified gamma distribution. As such, the p index is not directly comparable to the drop size spectra developed here. However, the parameters of Considine and Curry's drop size distribution are vertical velocity variance, temperature, pressure, the lapse rate in the cloud, and the lapse rate of a rising parcel. These parameters include essentially the same meteorological variables used in the drop size spectra developed here. Considine and Curry's results implied that if the lapse rate within the cloud is equal to the saturated adiabatic lapse rate, then the spectrum becomes infinitely narrow, approaching a monomodal distribution. This is consistent with our result that a cloud with adiabatic liquid water content will have an infinitely narrow spectrum and the spectrum will not be influenced by turbulent motions. Considine and Curry also found that the drop size spectra broadens as the vertical velocity variance increases, which is consistent with our results. This general agreement with Considine and Curry supports some of the assumptions used in their derivation. However, the present derivation provides a sounder theoretical justification for some of these assumptions. The drop size distribution developed here is easier to apply, since that derived by Considine and Curry requires knowledge of the parcel lapse rate that depends on the supersaturation ratio (which is not easily determined).

One of the most important quantities that characterizes the effect of turbulence on the size spectra is the relative dispersion $\sigma_r = (1 + p)^{-1/2}$. Its vertical profiles calculated with the values of $\tilde{p}_1$ from Fig. 6 are given in Fig. 8 for the four cases considered above. The dispersion for the cases with $w_{\mathrm{dyn}} = 10$–$15\ \mathrm{cm\ s^{-1}}$ decreases from 0.45–0.6 above cloud base to 0.3–0.4; that is, the size spectra in low stratus are narrowing with height above cloud base. These values are in good agreement with many observations, but the dispersions with $w_{\mathrm{dyn}} = 1\ \mathrm{cm\ s^{-1}}$ are 0.55–0.85, much larger than those observed locally. Note that the effect of decrease of σ_r upward is opposite to that observed above the base in convective clouds where dispersions increase upward (Warner 1969a); however, it is in a good agreement with the observation in stratus clouds (Noonkester 1984; Curry 1986) and in the upper halves of some convective clouds (e.g., Austin et al. 1985). The data from Table 4 show that the relative dispersions have maxima near cloud top and bottom and minimum in the middle cloud, near the maximum of q_L. The calculated values of σ_r are similar to the measured values shown in Table 4.

The indices $\tilde{p}_1$ corresponding to the asymptotic solution (2.20) characterize the breadth of the size spectra only in the lower layer, while the indices p can serve as a measure of the spectral breadth in the whole cloud. The dispersions calculated with the indices p from Fig. 5 are shown in Fig. 9. These dispersions exhibit minima of 0.2–0.3 near maximum values of q_L, and asymmetry of σ_r in vertical with larger dispersions near the base than in the upper layer, in agreement with observations shown in Table 4.

Hence, the analytical solutions derived in section 2 provide an explanation of the observed dispersions in clouds along with their possible different behavior with height. We have to emphasize that these are only approximate estimations of the dispersions based on several simplifications. The more accurate evaluation of σ_r should be based on the numerical solution of the complete kinetic equation with more realistic account for the profiles of $k(z)$, gradients $\partial f/\partial z$, etc.

The technique described above can be used to study covariances of moments of the distribution function with various quantities as was done based on observations by Curry (1986). The simplest is the covariance of liquid water content, $\overline{q_L'}$, with vertical velocity. Using (3.24) (see Part I) for $\overline{u_i' f'}$ in the low-frequency approximation ($k_{ij}^n = k_{ij}$) and the assumption of horizontal homogeneity (only the term $\partial/\partial z$ is kept), multiplying it by $(4\pi/3)\rho_w r^3$, and integrating over radii, we obtain

$$\begin{aligned}\overline{q_L' u_3'} &= \frac{4\pi}{3}\rho_w \int_0^\infty r^3 \overline{u_3' f'}\, dr \\ &= \frac{4\pi}{3}\rho_w \int_0^\infty r^3 \left[-k\left(\frac{\partial f}{\partial z} + G\frac{\partial f}{\partial r}\right)\right] dr \\ &= -k\frac{\partial q_L}{\partial z} - \frac{4\pi}{3}\rho_w G \int_0^\infty r^3 \frac{\partial f}{\partial r}\, dr. \end{aligned} \tag{3.11}$$

The last integral in (3.11) is equal to $-3N\overline{r^2}$. Including the expression (3.9) for G, the covariance (3.11) is written as

$$\overline{q_L' u_3'} = k\left[\left(\frac{dq_L}{dz}\right)_{\text{ad}} - \left(\frac{dq_L}{dz}\right)\right]. \tag{3.12}$$

The expression (3.12) shows that covariance of q_L with vertical velocity should be positive for the cases when adiabatic gradient of q_L is greater than the vertical gradient of q_L and is negative for the reverse situation. The first situation is met almost always, which causes positive correlation. In particular, this positive correlation of q_L and vertical velocity was described by Curry (1986) based on observations in Arctic stratus, which means that vertical gradients of q_L were less than adiabatic, in accord with the present theory.

4. Summary

In Part I of this paper we derived a kinetic equation of stochastic condensation that accounts for the effects of turbulence on the condensation process and can be suitable for use in cloud models with explicit microphysics. In Part II, we have obtained an analytical solution to the stochastic kinetic equations in the form of a gamma distribution with parameters that can be related directly to atmospheric conditions. An analytical solution to the kinetic equation is obtained by making the following approximations: horizontal homogeneity, quasi-steady state, and parameterized profiles of turbulence coefficient, effective vertical velocity, and radiative heating. It is shown that two asymptotic solutions exist, near cloud boundaries and in the center of the cloud, where the general solutions can be simplified and converted into the simple gamma distributions. These results show that gamma distributions are not simply the best fit to the measured size spectra but rather a fundamental property of the condensation process in clouds in the turbulent atmosphere.

The index of the gamma distribution, p, derived in this paper determines the relative dispersions of the size spectra, $\sigma_r \sim (p + 1)^{-1/2}$, and thereby cloud optical properties and the rate of precipitation formation. These analytical solutions allow us to express p and σ_r through fundamental atmospheric parameters: atmospheric dynamics (the mean vertical velocity and turbulence diffusion coefficient), cloud properties (droplet concentration and mean droplet radius), and the fundamental atmospheric constants (evaporation heat L and specific heat c_p; dry and moist adiabatic temperature lapse rates γ_d, γ_s). The index p is proportional to the mean effective vertical velocity and inversely proportional to the turbulence coefficient.

Results from these solutions were compared with examples of stratus clouds observed in the Arctic (Curry 1986) and stratocumulus near the coast of California (Noonkester 1984). We explain the observed behavior of the relative dispersions of the observed spectra: decrease (narrowing the spectra) with height above the base, minimum in the middle of the cloud, and increase again near the cloud top. We note that these profiles of the dispersions are essentially different from the observations in cumulus clouds, which show an increase of the relative dispersions above the cloud base (e.g., Warner 1969a) and were considered for many years as the general law for all clouds. Application of the analytical solutions obtained here enable us to explain different behavior with height of σ_r in low stratus and stratocumulus clouds and in convective clouds.

The parameterization of cloud drop size distributions based on these analytical solutions provides a good basis for parameterization of cloud microphysical and optical properties for climate and weather forecast models. Using the results from this paper on the index p and relative dispersions one can see that the clouds or cloud layers with larger updrafts or stronger radiative cooling (larger p and smaller effective radius r_{ef}) have larger optical thickness and the cloud layers with stronger turbulence (smaller p and larger r_{ef}) have smaller optical thickness.

While the kinetic equation derived in Part I can be used in numerical cloud models, the analytical solutions can be used for parameterization of cloud drop size spectra in cloud models with bulk microphysics or in climate models where elements of such parameterizations are utilized. Such incorporation of the elements of the size spectra might be especially useful in the models that have q_L and the mean radius as prognostic or diagnostic variables and assume a gamma distribution-like size spectra for parameterization of the cloud and radiative processes (e.g., Fowler et al. 1996). Given the liquid water content and mean radius at some time step from the model, the third parameter of the gamma distribution, the index p, can be calculated using (3.3). Note that this evaluation of p should be done with some caution, because it requires appropriate parameterizations of the subgrid vertical velocity and precise advective schemes for liquid water content and other moments of the spectra with minimum numerical diffusion.

Note finally that only the simplest cases of the solutions have been investigated here and more effort is needed to estimate the impact of stochastic processes on condensation using both analytical and numerical solutions to the kinetic equation. The approach developed in this paper can be extended to crystalline (cirrus and diamond dust) and mixed-phase clouds. These issues will be addressed in future papers.

Acknowledgments. This research was supported by the Department of Energy Atmospheric Radiation Measurement Program and the NASA FIRE program. Comments on the manuscript from Branko Kosovic, Andrea Codd, and Geoffrey Considine are appreciated. Two anonymous reviewers are thanked for their useful discussions that greatly helped to improve the quality of the paper. Oleg Melnik and Dmitry Khvorostyanov are

thanked for their help in calculations. The assistance of Jody Norman, Olga Melnik, and Alexander Kats in preparation of the manuscript and drawing the figures is appreciated.

APPENDIX A

Moments of the Size Spectra and Properties of the Kummer Function

The spectral moments for the distribution functions given by (2.12) and (2.15) can be determined following Landau and Lifshits (1958) from

$$M^{(\upsilon)} = \int_0^\infty e^{-\lambda x} x^\upsilon F(\alpha,\ \gamma,\ \beta x)\ dx$$

$$= \Gamma(\upsilon + 1)\lambda^{-(\upsilon+1)} F\left(\alpha,\ \upsilon + 1,\ \gamma,\ \frac{\beta}{\lambda}\right), \quad \text{(A.1)}$$

where $\Gamma(x)$ is the Euler gamma function, and $F(\alpha, \beta, \gamma, x)$ is the Gaussian hypergeometric function. We obtain the following moments for the distribution function (2.12):

$$M^{(n)} = \int_0^\infty r^n f\ dr$$

$$= c_1\Gamma(p + n + 1)\left[\frac{\alpha}{G}(1 - \mu)\right]^{-(p+n+1)}$$

$$\times F\left(\frac{p}{2\mu}(1 + \mu), p + n + 1, p; -\frac{2\mu}{1 - \mu}\right), \quad \text{(A.2)}$$

and for (2.15)

$$M^{(n)} = \int_0^\infty r^n f\ dr$$

$$= c_2\Gamma(p + n + 1)\left[\frac{\alpha}{G}(1 + \mu)\right]^{-(p+n+1)}$$

$$\times F\left(\frac{p}{2\mu}(\mu - 1), p + n + 1, p, \frac{2\mu}{1 + \mu}\right). \quad \text{(A.3)}$$

For $n = 0$, $M^{(n)} = N$ and we obtain normalization constants c_1, c_2 (2.16), (2.17).

The numerical and asymptotic solutions can be obtained using the series of the Kummer function and Gaussian hypergeometric function:

$$F(\alpha, \gamma, x) = 1 + \frac{\alpha}{\gamma}\frac{x}{1!} + \frac{\alpha(\alpha + 1)}{\gamma(\gamma + 1)}\frac{x^2}{2!} + \cdots \quad \text{(A.4a)}$$

$$F(\alpha, \beta, \gamma, x) = 1 + \frac{\alpha\beta}{\gamma}\frac{x}{1!} + \frac{\alpha(\alpha + 1)\beta(\beta + 1)}{\gamma(\gamma + 1)}\frac{x^2}{2!} + \cdots, \quad \text{(A.4b)}$$

which converge for finite values of x (parameters α, β are arbitrary and parameter γ should not be a negative integer). Of additional use are the following asymptotic relations, which can be obtained from those given in Landau and Lifshits (1958) and from (A.4a,b):

$$\lim_{x\to\infty} F(\alpha, \gamma, x) \approx \frac{\Gamma(\gamma)}{\Gamma(\alpha)} e^x x^{\alpha-\gamma} \qquad F(0, \gamma, x) = 1 \quad \text{(A.5)}$$

$$\lim_{x\to 0} F(\alpha, \gamma, x) = 1 \qquad F(\alpha, \alpha, x) = e^x. \quad \text{(A.6)}$$

The gamma distribution $f(r) = \tilde{c}r^a \exp(-br)$ can be normalized to the droplet concentration N:

$$N = \int_0^\infty f(r)\ dr = \tilde{c}\int_0^\infty r^a e^{-br}\ dr$$

$$= (\tilde{c}/b^{a+1})\int_0^\infty x^a e^{-x}\ dx = (\tilde{c}/b^{a+1})\Gamma(a + 1),$$

$$\tilde{c} = N\frac{b^{a+1}}{\Gamma(a + 1)}. \quad \text{(A.7)}$$

Hence, for the gamma distribution with mean radius $\overline{r}$ and index p, the parameters $a = p$, $b = (p + 1)/\overline{r}$, and the drop size spectra are given by

$$f(r) = N\frac{(p + 1)^{p+1}}{\Gamma(p + 1)}\frac{1}{\overline{r}}\left(\frac{r}{\overline{r}}\right)^p \exp\left(-(p + 1)\frac{r}{\overline{r}}\right). \quad \text{(A.8)}$$

In applications, it is convenient to use moments $M^{(n)}$ of the drop size distribution, which can be expressed here through three parameters of gamma distribution: droplet concentration N, mean radius $\overline{r}$, and the index p;

$$M^{(n)} = \int_0^\infty r^n f(r)\ dr$$

$$= N\frac{(p + 1)^{p+1}}{\Gamma(p + 1)}\int_0^\infty \left(\frac{r}{\overline{r}}\right)^p \exp\left(-(p + 1)\frac{r}{\overline{r}}\right) d\left(\frac{r}{\overline{r}}\right)$$

$$= N\frac{\Gamma(p + 1 + n)}{\Gamma(p + 1)}\left(\frac{\overline{r}}{p + 1}\right)^n. \quad \text{(A.9)}$$

In particular, we see that $M^{(0)} = N$. The next three moments can be simplified by using the recurrent relation for the Eulerian gamma function, $\Gamma(x + 1) = x\Gamma(x)$:

$$M^{(1)} = N\overline{r}, \qquad M^{(2)} = \frac{p + 2}{p + 1}N\overline{r}^2,$$

$$M^{(3)} = N\overline{r}^3\frac{(p + 2)(p + 3)}{(p + 1)^2}. \quad \text{(A.10)}$$

In some applications, it is convenient to use modal radius r_m, which can be determined from the condition $df(r_m)/dr = 0$, and the effective radius used in radiative calculations, r_{ef}, which can be expressed as the relation

of the third to the second moments. Using the above relationships, it is easily shown that

$$\bar{r} = \frac{p+1}{p} r_m, \qquad r_{\text{ef}} = \frac{M^{(3)}}{M^{(2)}} = \frac{p+3}{p+1}\bar{r},$$

$$r_{\text{ef}} = \frac{p+3}{p+1}\bar{r} = \frac{p+3}{p} r_m. \tag{A.11}$$

The expression for the dispersion of the spectra can be evaluated from the zeroth, first, and second moments with use of (A.10):

$$\sigma_d^2 = \frac{1}{N}\int_0^\infty f(r-\bar{r})^2\, dr = \frac{1}{N}(M^{(2)} - 2\bar{r}M^{(1)} + \bar{r}^2 M^{(0)})$$

$$= \bar{r}^2/(p+1). \tag{A.12}$$

APPENDIX B

List of Symbols

c_1, c_2	Normalization factors for size spectra
c_p	Specific heat capacity
D	Water vapor diffusion coefficient
c	Coefficient of regular condensation, (2.1a)
$F(a, b; z)$	Kummer's confluent hypergeometric function
$F(a, b, c; z)$	Gaussian hypergeometric function
f	Droplet size distribution function
G	Parameter defined in (3.13)
k_{ij}, k	Components of turbulence coefficient
L	Latent heat of condensation
N	Droplet concentration
p	Indices of gamma distribution
$\tilde{p}_1$, $\tilde{p}_2$	Indices of asymptotic solutions (2.20), (2.21)
Q_{rad}	Radiative temperature change
q	Specific humidity
q_s	Saturation specific humidity
q_L	Liquid water content
$q_{L,\text{ad}}$	Adiabatic liquid water content
r	Droplet radius
$\bar{r}$	Mean radius
r_m	Modal radius
r_{ef}	Effective radius
$\dot{r}$	Droplet growth rate
$S = \rho_v - \rho_s$	Supersaturation
t	Time
T	Temperature
$v(r)$	Terminal velocity
w	Vertical velocity
w_{rad}	Radiative-effective velocity
w_{ef}	Effective vertical velocity
x, y, z	Coordinates
γ_d, γ_s	Dry and moist adiabatic lapse rates
$\alpha(z)$	Relative gradient of distribution function
β	Exponent of gamma distribution, (2.7)
$\Gamma(x)$	Euler gamma function
$\delta(x)$	Dirac delta function
δ_{ij}	Kronecker symbol
$\varepsilon - c$	Condensation rate
μ	Coefficient in exponent of gamma distribution, (2.7)
ρ_v, ρ_w, ρ_a	Densities of vapor, water, and air
σ_r	Relative spectral dispersion
τ_f	Supersaturation relaxation time
ω	Turbulent frequency
ω_p	Frequency of supersaturation relaxation

REFERENCES

Ackerman, S. A., and G. L. Stephens, 1987: The absorption of solar radiation by cloud droplets: An application of anomalous diffraction theory. *J. Atmos. Sci.,* **44,** 1574–1588.

Aleksandrov, E. L., and K. B. Yudin, 1979: On the vertical profile of the cloud microstructure in stratiform clouds. *Sov. Meteor. Hydrol.,* **12,** 47–61.

Austin, P. H., M. B. Baker, A. M. Blyth, and J. B. Jensen, 1985: Small-scale variability in warm continental cumulus clouds. *J. Atmos. Sci.,* **42,** 1123–1138.

Baker, M. B., R. E. Briedenthal, T. W. Choularton, and J. Latham, 1984: The effects of turbulent mixing in clouds. *J. Atmos. Sci.,* **41,** 299–304.

Bartlett, J. T., and P. R. Jonas, 1972: On the dispersions of the sizes of droplets growing by condensation in turbulent clouds. *Quart. J. Roy. Meteor. Soc.,* **98,** 150–164.

Considine, G., and J. A. Curry, 1996: A statistical model of drop size spectra for stratocumulus clouds. *Quart. J. Roy. Meteor. Soc.,* **122,** 611–634.

Cotton, W. R., and R. A. Anthes, 1989: *Storm and Cloud Dynamics.* Academic Press, 883 pp.

Curry, J. A., 1986: Interactions among turbulence, radiation and microphysics in Arctic stratus clouds. *J. Atmos. Sci.,* **43,** 525–538.

——, E. E. Ebert, and G. F. Herman, 1988: Mean and turbulent structure of the summertime Arctic cloudy boundary layer. *Quart. J. Roy. Meteor. Soc.,* **114,** 715–746.

Deirmendijan, D., 1969: *Electromagnetic Scattering on Spherical Polydispersions.* Elsevier, 291 pp.

Dmitrieva-Arrago, L. R, and I. V. Akimov, 1998: A method for calculation of nonconvective precipitation on the basis of liquid water content forecast with account for cloud microphysics. *Sov. Meteor. Hydrol.,* **11,** 47–59.

Feingold, G., B. Stevens, W. R. Cotton, and R. L. Walko, 1994: An explicit cloud microphysics/LES model designed to simulate the Twomey effect. *Atmos. Res.,* **33,** 207–233.

Fowler, L. D., D. A. Randall, and S. A. Rutledge, 1996: Liquid and ice cloud microphysics in the CSU general circulation model. Part I: Model description and simulated microphysical processes. *J. Climate,* **9,** 489–529.

Herman, G. F., and J. A. Curry, 1984: Observational and theoretical studies of solar radiation in Arctic stratus clouds. *J. Climate Appl. Meteor.,* **23,** 5–24.

Heymsfield, A. J., and C. M. R. Platt, 1984: A parameterization of the particle size spectrum of ice clouds in terms of the ambient temperature and the ice water content. *J. Atmos. Sci.,* **41,** 846–855.

Khvorostyanov, V., 1995: Mesoscale processes of cloud formation, cloud-radiation interaction and their modelling with explicit cloud microphysics. *Atmos. Res.* **39,** 1–67.

——, and J. A. Curry, 1999: Toward the theory of stochastic condensation in clouds. Part I: A general kinetic equation. *J. Atmos. Sci.,* **56,** 3985–3996.

Landau, L. D., and E. M. Lifshitz, 1958: *Quantum Mechanics, Non-Relativistic Theory. Vol. 3, Course of Theoretical Physics,* J. B. Sykes and J. S. Bell, Translators, Addison-Wesley, 526 pp.

Levin, L. M., and Y. S. Sedunov, 1966: Stochastic condensation of drops and kinetics of cloud spectrum formation. *J. Rech. Atmos.*, **2,** 425–432.

Manton, M. J., 1979: On the broadening of a droplet distribution by turbulence near cloud base. *Quart. J. Roy. Meteor. Soc.*, **105,** 899–914.

Mason, B. J., 1971: *Physics of Clouds.* Clarendon Press, 481 pp.

Matveev, L. T., 1984: *Cloud Dynamics.* D. Reidel, 421 pp.

Mitchell, D. L., and W. P. Arnott, 1994: A model predicting the evolution of ice particle size spectra and radiative properties of cirrus clouds. Part II: Dependence of absorption and extintion on ice crystal morphology. *J. Atmos. Sci.,* **51,** 817–832.

Noonkester, V. R., 1984: Droplet spectra observed in marine stratus cloud layers. *J. Atmos. Sci.,* **41,** 829–845.

Pruppacher, H. R., and J. D. Klett, 1997: *Microphysics of Clouds and Precipitation.* 2d ed., Kluwer, 997 pp.

Ryan, B. F., 1996: On the global variation of precipitating layer clouds. *Bull. Amer. Meteor. Soc.*, **77,** 53–70.

Sedunov, Y. S., 1974: *Physics of Drop Formation in the Atmosphere.* Wiley, 234 pp.

Smirnov, V. I., and L. A. Nadeykina, 1986: On the theory of the drop size spectrum formed by condensation in turbulent cloud. *Izv. Acad. Sci. USSR, Atmos. Oceanic Phys.,* **22,** 478–487.

Stepanov, A. S., 1975: Condensational growth of cloud droplets in a turbulized atmosphere. *Izv. Akad. Sci. USSR, Atmos. Oceanic Phys.,* **11,** 27–42.

Stephens, G. L., S. C. Tsay, P. W. Stackhouse, and P. J. Flatau, 1990: The relevance of microphysical and radiative propserties of cirrus clouds to climate and climate feedback. *J. Atmos. Sci.,* **47,** 1742–1753.

Tsay, S. C., and K. Jayaweera, 1984: Physical characteristics of Arctic Stratus clouds. *J. Climate Appl. Meteor.,* **23,** 584–596.

Voloshchuk, V. M., and Y. S. Sedunov, 1977: A kinetic equation for the evolution of the droplet spectrum in a turbulent medium in the condensation state of cloud development. *Sov. Meteor. Hydrol.,* **3,** 3–14.

Warner, J., 1969a: The microstructure of cumulus cloud. Part I. General features of the droplet spectrum. *J. Atmos. Sci.,* **26,** 1049–1059.

——, 1969b: The microstructure of cumulus cloud. Part II. The effect on droplet size distribution of the cloud nucleus spectrum and vertical velocity. *J. Atmos. Sci.,* **26,** 1272–1282.